DRAFT VERSION JANUARY 10, 2018
Preprint typeset using LaTeX style emulateapj v. 5/2/11

KMT-2015-1b: A GIANT PLANET ORBITING A LOW-MASS DWARF HOST STAR DISCOVERED BY A NEW HIGH-CADENCE MICROLENSING SURVEY WITH A GLOBAL TELESCOPE NETWORK

K.-H. HWANG[1], C. HAN[1,*], J.-Y.CHOI[1], H. PARK[1], Y. K. JUNG[1], I.-G. SHIN[1], M. D. ALBROW[2], A. GOULD[3], V. BOZZA[4,5], B.-G. PARK[6], S.-L. KIM[6], C.-U. LEE[6], S.-M. CHA[6,7], D.-J. KIM[6] AND Y. LEE[6,7]

[1]Department of Physics, Chungbuk National University, Cheongju 361-763, Republic of Korea
[2]University of Canterbury, Department of Physics and Astronomy, Private Bag 4800, Christchurch 8020, New Zealand
[3]Department of Astronomy, Ohio State University, 140 W. 18th Ave., Columbus, OH 43210, USA
[4]Dipartimento di Fisica "E. R. Caianiello", Universit'a di Salerno, Via Giovanni Paolo II, 84084 Fisciano (SA), Italy
[5]Istituto Nazionale di Fisica Nucleare, Sezione di Napoli, Via Cintia, 80126 Napoli, Italy
[6]Korea Astronomy and Space Science Institute, Daejon 305-348, Republic of Korea
[7]School of Space Research, Kyung Hee University, Yongin 446-701, Republic of Korea and
[*]Corresponding author

Draft version January 10, 2018

ABSTRACT

We report the discovery of an extrasolar planet, KMT-2015-1b, that was detected using the microlensing technique. The planetary lensing event was observed by KMTNet survey that has commenced in 2015. With dense coverage by using network of globally distributed telescopes equipped with very wide-field cameras, the short planetary signal is clearly detected and precisely characterized. We find that KMT-2015-1b is a giant planet orbiting a low-mass M-dwarf host star. The planet has a mass about twice that of Jupiter and it is located beyond the snow line of the host star. With the improvement of existing surveys and the advent of new surveys, future microlensing planet samples will include planets not only in greatly increased number but also in a wide spectrum of hosts and planets, helping us to have a better and comprehensive understanding about the formation and evolution of planets.

Subject headings: gravitational lensing: micro – planetary systems

1. INTRODUCTION

Since the first discovery by Wolszczan & Frail (1992) followed by Mayor & Queloz (1995), many exo-planets have been discovered. With the *Kepler* mission, the number of known planets explosively increased and now reaches $\sim$2000. Most of them were discovered by either the transit or radial-velocity methods.

Although relatively few, planets have also been discovered using the microlensing method. Due to the fact that these planetary systems are detected through their gravitational fields rather than their radiation, this method makes it possible to detect planets around faint stars and even dark objects. Furthermore, microlensing is sensitive to planets on wide orbits beyond the snow line, which separates regions of rocky planet formation from regions of icy planet formation, while other major planet detection techniques are sensitive to close-in planets. Being able to detect planets that are difficult to be detected by other techniques, the method is important for the comprehensive understanding of planet formation (Gaudi 2012).

One of the important reasons for the small number of microlensing planets is the difficulty of observation. The planetary signal of a microlensing planet is a short-term perturbation to the smooth lensing light curve induced by the host star (Mao & Paczynski 1991; Gould & Loeb 1992). To detect short planetary signals, the previous generation of lensing experiments applied a strategy where lensing events were detected by wide-field surveys and events detected by surveys were intensively monitored using multiple narrow-field telescopes (Albrow et al. 1998). However, the limited number of follow-up telescopes makes it difficult to intensively monitor all alerted events, which number reaches several hundreds at a given moment. As a result, the detection efficiency of microlensing planets has been low.

In this paper, we report the discovery of a giant planet KMT-2015-1b orbiting a low-mass M dwarf. The planetary lensing event was observed by a new survey that achieves round-the-clock coverage of lensing events with a high cadence by using global network of telescopes equipped with very wide-field cameras.

The paper is organized as follows. In Section 2, we describe the observation of the planetary microlensing event by the new lensing survey, including instrument, data acquisition and reduction process. In Section 3, we give a description of the modeling procedure conducted to analyze the observed lensing light curve. We provide the estimated physical parameters of the discovered planetary system in Section 4. Finally, we summarize the result and make a brief discussion about the result in Section 5.

2. OBSERVATION

The planet was discovered from the observation of a microlensing event that occurred on a star located toward the Galactic bulge field. The equatorial coordinates of the lensed star (source) are (RA,DEC) = ($17^{\rm h}58^{\rm m}39^{\rm s}.01$,$-28^\circ01'54''.1$), that correspond to the Galactic coordinates (l,b) = (2.24°,–2.00°). The lensing-induced brightening of the source star was noticed in early February, 2015 by the OGLE (Udalski et al. 2015) survey and lasted for about a month, during which the bulge field can be seen for less than an hour per night.

The event was also observed by the KMTNet (Korea Microlensing Telescope Network) lensing survey that started its test observation in February, 2015, which matches the occurrence time of the event. The event was dubbed as KMT-2015-BLG-0048 in the KMT event list. The survey uses three identical telescopes that are located at Cerro Tololo Interameri-

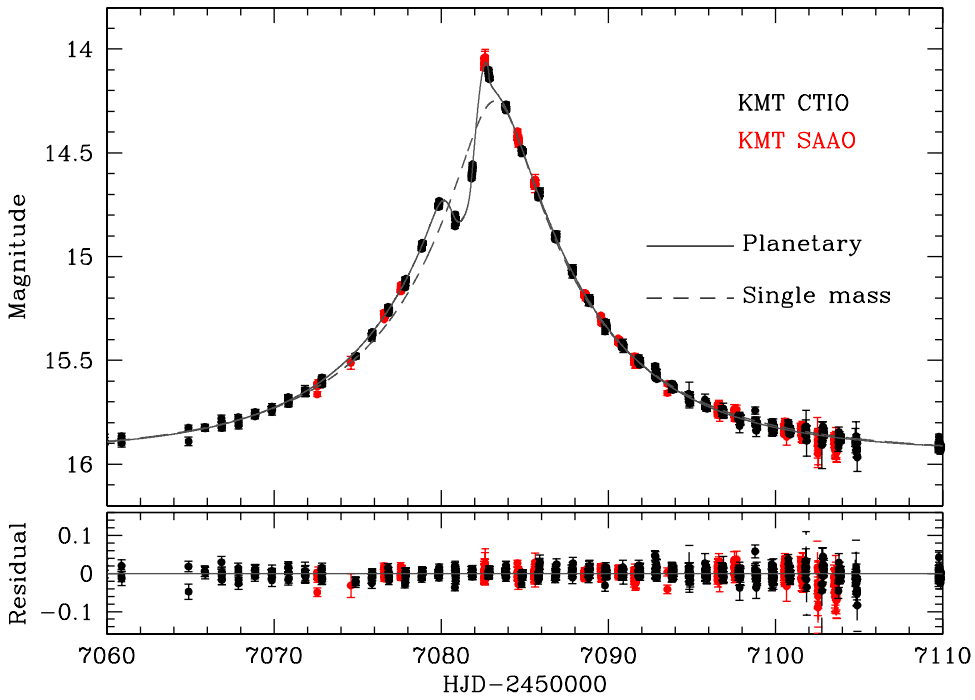

FIG. 1.— Light curve of the microlensing event KMT-2015-BLG-0048. Solid and dashed curves represent the best-fit models from binary (planetary) and single-mass lens modeling, respectively.

can Observatory, Chile (KMT CTIO), South African Astronomical Observatory, South Africa (KMT SAAO), and Siding Spring Observatory, Australia (KMT SSO). At the time of the event, KMT SSO was not online and the event was observed by two telescopes, KMT CTIO and KMT SAAO. Each telescope has a 1.6m aperture and is equipped with a mosaic camera composed of four 9K×9K CCDs. Each CCD has a pixel size of 10 microns corresponding to 0.4 arcsec/pixel and thus the camera has 4 deg^2 field of view (Kim et al. 2015). With the global network of wide-field telescopes that are separated by ∼8 hrs in longitudes, the survey continuously observes the Galactic bulge field with a cadence of 1 observation every 10 minutes. Images were taken in Johnson-Cousin I and V bands. From the observation of the event, we acquired 786 I-band and 54 V-band images from KMT CTIO and 1117 I-band images from KMT SAAO observations. We note that I-band data are used to analyze the lensing event and V-band data are used to constrain the source star.

Photometry of the images were conducted using a customized pipeline that is based on the difference image analysis code of Albrow et al. (2009) Since data are taken by the different telescopes and photometry based on an automated pipeline often results in inaccurate error estimation, we renormalize error bars of the individual data sets by

$$\sigma' = k(\sigma_0^2 + \sigma_{\rm min}^2)^{1/2}, \quad (1)$$

where σ_0 is the error estimated from the pipeline, $\sigma_{\rm min}$ is a factor used to make the cumulative distribution function of χ^2 as a function of lensing magnification linear, and k is a scaling factor to make χ^2 per degree of freedom (dof) become unity. We note that the factor $\sigma_{\rm min}$ is required to ensure that each data set is fairly weighted according to its error bars.

In Figure 1, we present the light curve of KMT-2015-BLG-0048. Compared to the continuous and symmetric light curve of a single-mass event, the light curve exhibits a short-term perturbation during $7080.0 \lesssim {\rm HJD}-2450000 \lesssim 7082.5$. The perturbation shows a feature that is composed of a depression centered at HJD − 2450000 ∼ 7081.5 and brief bumps at both edges of the depression. Such dips, usually surrounded by two bumps, are a generic feature of lensing systems with small mass ratios $q \ll 1$ with normalized planet-star separations $s < 1$, i.e., planets inside the Einstein ring. This is because the star's gravity generates two images, one inside and the other outside the Einstein ring. The former, being a saddle point on the time delay surface, is easily suppressed if the planet lies in or near the path, thereby causing relative demagnification, and hence a dip in the light curve. To be noted is that the major structure of the anomaly feature was well covered by the survey observation despite the short time window each night toward the field.

TABLE 1
LENSING PARAMETERS

Parameters	Values
χ^2/dof	1896/1896
t_0 (HJD)	2457083.081 ± 0.004
u_0	0.221 ± 0.003
$t_{\rm E}$ (days)	10.90 ± 0.10
s	0.955 ± 0.003
q (10^{-3})	6.84 ± 0.18
α (rad)	5.352 ± 0.003
ρ (10^{-3})	44.7 ± 0.8

3. ANALYSIS

Keeping in mind that the anomaly pattern is likely to be produced by a binary lens with a low mass ratio, we conduct binary-lens modeling. Basic binary-lens modeling requires at least 9 parameters, including 7 principal parameters for the lensing system and 2 flux parameters for each observatory. The first 3 of the principal parameters describe the source approach with respect the lens, including the time of the closest source approach to the reference position of the lens, t_0, the

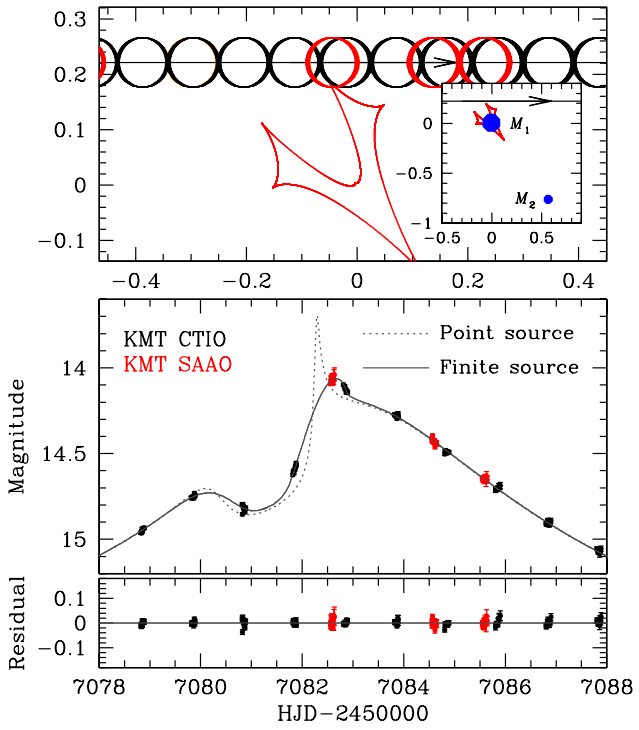

FIG. 2.— Lens system geometry. The upper panel shows the source trajectory (straight line with an arrow) with respect to the lens components (marked by M_1 and M_2) and caustics (closed concave curve) and the lower panel shows the light variation with the progress of the source position. Lengths are scaled to the Einstein radius and the source trajectory is aligned so that the progress of the source matches the light curve shown in the lower panel. The inset in the upper panel shows the wide view and the major panel shows the enlarged view around the caustic. The empty circles on the source trajectory represent the source positions at the times of observation and the size indicates the source size. The dotted curve in the lower panel is the light curve expected for a point source.

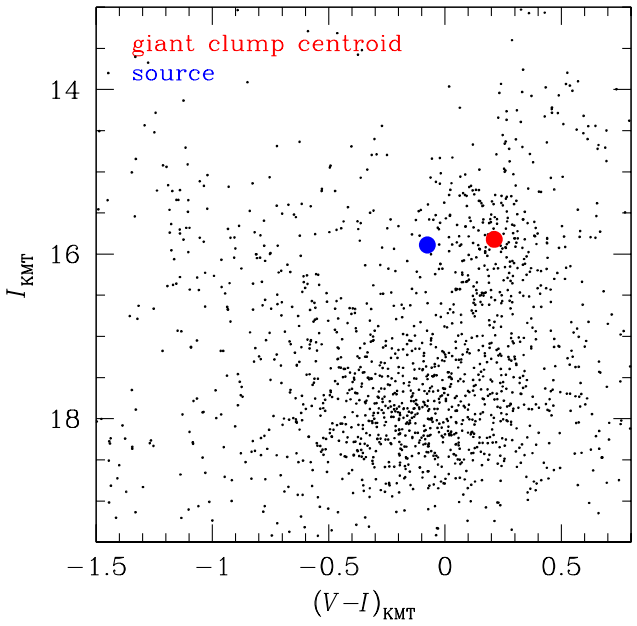

FIG. 3.— Source position in the instrumental color-magnitude diagram of nearby stars with respect to the centroid of the giant clump.

lens-source separation at that moment, u_0 (impact parameter), and the time for the source to cross the angular Einstein radius $\theta_{\rm E}$ of the lens, $t_{\rm E}$ (Einstein time scale). For the reference position of the lens, we use the center of mass. The other 3 principal parameters describe the lens binarity including the projected separation s and the mass ratio q between the binary components, and the angle between the source trajectory and the binary axis, α. We note that the impact parameter u_0 and the binary separation s are normalized by $\theta_{\rm E}$. The other parameter defined as the ratio of the angular source radius to the Einstein radius, $\rho = \theta_*/\theta_{\rm E}$, is needed to describe light curve deviations affected by finite-source effects.

For some lensing events, the basic parameters are not adequate to precisely describe observed lensing light curves. The known causes of such deviations include the parallax effect (Gould 1992) and the lens orbital effect (Albrow et al. 2000; An et al. 2002; Jung et al. 2013). The parallax effect is caused by the deviation of the observer's motion from rectilinear due to the orbital motion of the Earth around the Sun. On the other hand, the lens-orbital effect is caused by the orbital motion of the lens. Such effects are important for long time-scale events for which the orbital motion of the Earth and/or lenses are important. For KMT-2015-BLG-0048, which lasted for $\sim$1 month, we find that these higher-order effects are negligible.

Modeling the light curve proceeded in several steps. First, we conduct thorough a grid search for solutions in the parameter space of (s, q, α), for which lensing light curves vary sensitively to the change of the parameters. In this process, other parameters are searched for by using a downhill approach. Second, we investigate all possible local solutions in the parameter space in order to check the existence of degenerate solutions where different combinations of the lensing parameters result in a similar light curve. Finally, we search for the global solution by comparing χ^2 values of the identified local solutions. For the downhill χ^2 minimization, we use the Markov Chain Monte Carlo (MCMC) method.

From the search for a solution, we find that the event was produced by a planetary system where the planet/host mass ratio is $q = 6.84 \times 10^{-3}$ and the projected planet-host separation, $s = 0.96$, is slightly less than the Einstein radius of the lens. In Table 1, we present the best-fit lensing parameters, where the error bars are estimated from the scatter of the MCMC chain. In Figure 2, we present the geometry of the lens system corresponding to the solution. Due to the resonance of the projected separation to $\theta_{\rm E}$, i.e. $s \sim 1$, the lens system forms a single large caustic around the host of the planet. The source passed the backside of the arrowhead-shaped caustic. The depression in the light curve occurred when the source was in the demagnification valley between the two protrudent cusps that caused the brief bumps on both sides of the depression. The source crossed the tip of one of the cusps during which the light curve shows a clear finite-source signature from which we accurately measure the normalized source radius ρ. To be noted is that the measured value of $\rho = 44.7 \times 10^{-3}$ is significantly larger than typical values $\sim 10^{-3}$ for main-sequence and $\sim 10^{-2}$ for giant source stars. For a given size of a bulge star, this suggests that the Einstein radius is very small.

Since finite-source effects are clearly detected, it is possible to determine the angular Einstein radius. The Einstein radius is determined by $\theta_{\rm E} = \theta_*/\rho$. The normalized source radius ρ is measured from the analysis of the light curve around the planetary perturbation. The angular radius of the source star, θ_*, is determined from its de-reddened color $(V-I)_0$ and brightness I_0. To measure color and brightness, we locate the source star in the instrumental(uncalibrated) color-magnitude diagram of neighboring stars in the same field and

calibrate the color and brightness based on the location of the centroid of the giant clump (GC), for which its de-reddened color $(V-I)_{0,\rm GC}$ and brightness $I_{0,\rm GC}$ are known to be constant and thus can be used as a standard candle. Figure 3 shows the locations of the source and giant clump centroid in the instrumental color-magnitude diagram. By adopting $(V-I)_{0,\rm GC} = 1.06$ (Bensby et al. 2011) and brightness $I_{0,\rm GC}$ accounting for variation with Galactic longitude (Nataf et al. 2013), we find that $(V-I, I)_0 = (0.78, 14.5)$, indicating that the source is a G-type giant star. We then convert $V-I$ into $V-K$ using the color-color relation of Bessell & Brett (1988) and finally determine θ_* using the color-angular radius relation of Kervella et al. (2004). We find that the angular source radius is $\theta_* = 4.39 \pm 0.56\ \mu$as. Then the angular Einstein radius is

$$\theta_{\rm E} = 0.098 \pm 0.013\ {\rm mas}. \quad (2)$$

Combined with the Einstein time scale estimated from lens modeling, the relative lens-source proper motion is determined as

$$\mu = \frac{\theta_{\rm E}}{t_{\rm E}} = 3.29 \pm 0.43\ {\rm mas\ yr^{-1}}. \quad (3)$$

As expected, the estimated Einstein radius is substantially smaller than ~ 0.5 mas for typical Galactic microlensing events.

4. PHYSICAL PARAMETERS

For the unique determination of the mass M and distance D_L to the lens, it is required to simultaneously measure both the lens parallax and the Einstein radius (Gould 1992). Nevertheless, the above measurements of the Einstein radius $\theta_{\rm E}$ and the proper motion μ can be combined with a Galactic model to statistically constrain M and D_L via a Bayesian analysis. We use the Han & Gould (1995) model, whose matter distribution is based on a double-exponential disk and a triaxial bulge. The disk velocity distribution is assumed to be Gaussian about the rotation velocity and the bulge velocity distribution is a triaxial Gaussian with components deduced from the flattening via the tensor virial theorem. The mass function is based on *Hubble Space Telescope* star counts.

The results of this Bayesian analysis

$$M = 0.18 \pm 0.12\ M_\odot; \qquad D_L = 8.2 \pm 0.9\ {\rm kpc} \quad (4)$$

can be easily understood based on simple physical reasoning. First, the Enstein radius is by definition the root-mean-square to the lens mass and the lens-source relative parallax $\pi_{\rm rel}$, i.e.

$$\theta_{\rm E} = \sqrt{\kappa M \pi_{\rm rel}}; \qquad \kappa = \frac{4G}{c^2 {\rm AU}} \simeq 8.1 \frac{\rm mas}{M_\odot}. \quad (5)$$

Because $\theta_{\rm E} = 0.098$ mas is unusually small, either M or $\pi_{\rm rel}$ should be small: $(M/M_\odot)(\pi_{\rm rel}/\mu{\rm as}) = 1.2$. Thus, if the lens is a star ($M > 0.08\ M_\odot$), it is $\pi_{\rm rel} < 15\ \mu$as and so lies in the Galactic bulge. This, combined with the fact that the Galactic density profile along the line of sight peaks strongly in the bulge, heavily favors bulge lenses. Finally, the measured proper motion is very typical of bulge lenses, but only half the size of typical proper motions.

In principle, the lens could be a star of any mass in the bulge. However, the measurement of $\theta_{\rm E}$ telles us that if it were a solar mass star, then $\pi_{\rm rel} = 1.2\ \mu$as, which would imply a distance from lens to source of only $D_S - D_L = 70$ pc. It is this small amount of available phase space for heavier lenses that drive the Bayesian estimate toward low mass lenses.

The measurement of q from the lens model then directly yields an estimate of the planet mass

$$M_p = qM = 2.2 \pm 1.4\ M_J, \quad (6)$$

while the measurement of s yields the projected lens-host separation

$$d_\perp = sD_L\theta_{\rm E} = 0.76 \pm 0.08\ {\rm AU}. \quad (7)$$

Considering the low temperature of the host star, the planet is located beyond the ice line.

5. SUMMARY AND DISCUSSION

We reported the discovery of an extrasolar planet KMT-2015-1b that was detected by using the microlensing technique. The planetary lensing event was observed by the KMTNet survey that has commenced in 2015. Despite the short time window in the early bulge season, unambiguous detection and precise characterization of the planetary system was possible due to the dense coverage of the planet-induced perturbation by using network of globally distributed telescopes equipped with very wide-field cameras. We find that KMT-2015-1b is a giant planet orbiting a low-mass M-dwarf host star. The planet has a mass about twice that of the Jupiter and it is located beyond the snow line of the host star.

Cool M dwarfs far outnumber sun-like stars and thus understanding the process of planet formation around them is important. Furthermore, small masses and low luminosities of M dwarfs provide leverage on conditions of planet formation, enabling to check the validity of existing formation theories and refine survived theories. With the improvement of existing surveys and the advent of new surveys, future microlensing planet sample will include planets not only in greatly increased number but also in wide spectrum of hosts and planets, helping us to have better and comprehensive understanding about the formation and evolution of planets.

Work by C.H. was supported by Creative Research Initiative Program (2009-0081561) of National Research Foundation of Korea. Work by A.G. was supported by NASA grant NNXRAB99G. This research has made the telescopes of KMTNet operated by the Korea Astronomy and Space Science Institute (KASI). We acknowledge the high-speed internet service (KREONET) provided by Korea Institute of Science and Technology Information (KISTI)

REFERENCES

Albrow, M., Beaulieu, J.-P., Birch, P., et al. 1998, ApJ, 509, 687
Albrow, M. D., Beaulieu, J.-P., Caldwell, J. A. R., et al. 2000, ApJ, 534, 894
Albrow, M. D., Horne, K., Bramich, D. M., et al. 2009, MNRAS, 397, 2099
An, J. H., Albrow, M. D., Beaulieu, J.-P., et al. 2002, ApJ, 572, 521
Bensby, T., Adén, D., Meléndez, J., et al. 2011, A&A, 533, A134
Bessell, M. S., & Brett, J. M. 1988, PASP, 100, 1134
Gaudi, B. S. 2012, ARA&A, 50, 411
Gould, A. 1992, ApJ, 392, 442
Gould, A., & Loeb, A. 1992, ApJ, 396, 104
Han, C., & Gould, A. 1995, ApJ, 447, 53
Jung, Y. K., Han, C., Gould, A., & Maoz, D. 2013, ApJ, 768, L7J
Kervella, P., Bersier, D., Mourard, D., et al. 2004, A&A, 428, 587
Kim, S.-L., Lee, C.-U., Park, B.-G., et al. 2015, Journal of the Korean Astronomical Society, in preparation
Mao, S., & Paczynski, B. 1991, ApJ, 374, L37
Mayor, M., & Queloz, D. 1995, Nature, 378, 355

Nataf, D. M., Gould, A., Fouqué, P., et al. 2013, ApJ, 769, 88
Udalski, A., Szymański, M. K., & Szymański, G. 2015, Acta Astron., 65, 1
Wolszczan, A., & Frail, D. A. 1992, Nature, 355, 145